MASSIVE STARS - NUCLEOSYNTHESIS

- $m \gtrsim 11 m_\odot$

  $< 11 m_\odot \rightarrow$ AGB $\rightarrow$ WD (CO)
  SAGB (ONe)

  (Z dep.?

- ENDS AS SN II, SNIb, SNIc
  - H spec.
  - No H spec
    - $\dot{m} \rightarrow$ STRIPPED CORE

- MAJOR n's CONTRIBUTOR
  - FEW MASSIVE STARS BUT EFFICIENT IN PROCESSING & EJECTING LARGE FRACTION OF MASS & EXPOSURE TO HIGH T/ρ IN BOTH HYDROSTATIC & EXPLOSIVE BURNING
  - SOME KEY GAPS AMONG (LiBeB) (^{15}N....) (s-process) (r-process?)
  - $m \sim 25 M_\odot$ OFTEN TAKEN AS REPRESENTATIVE OF A GENERATION

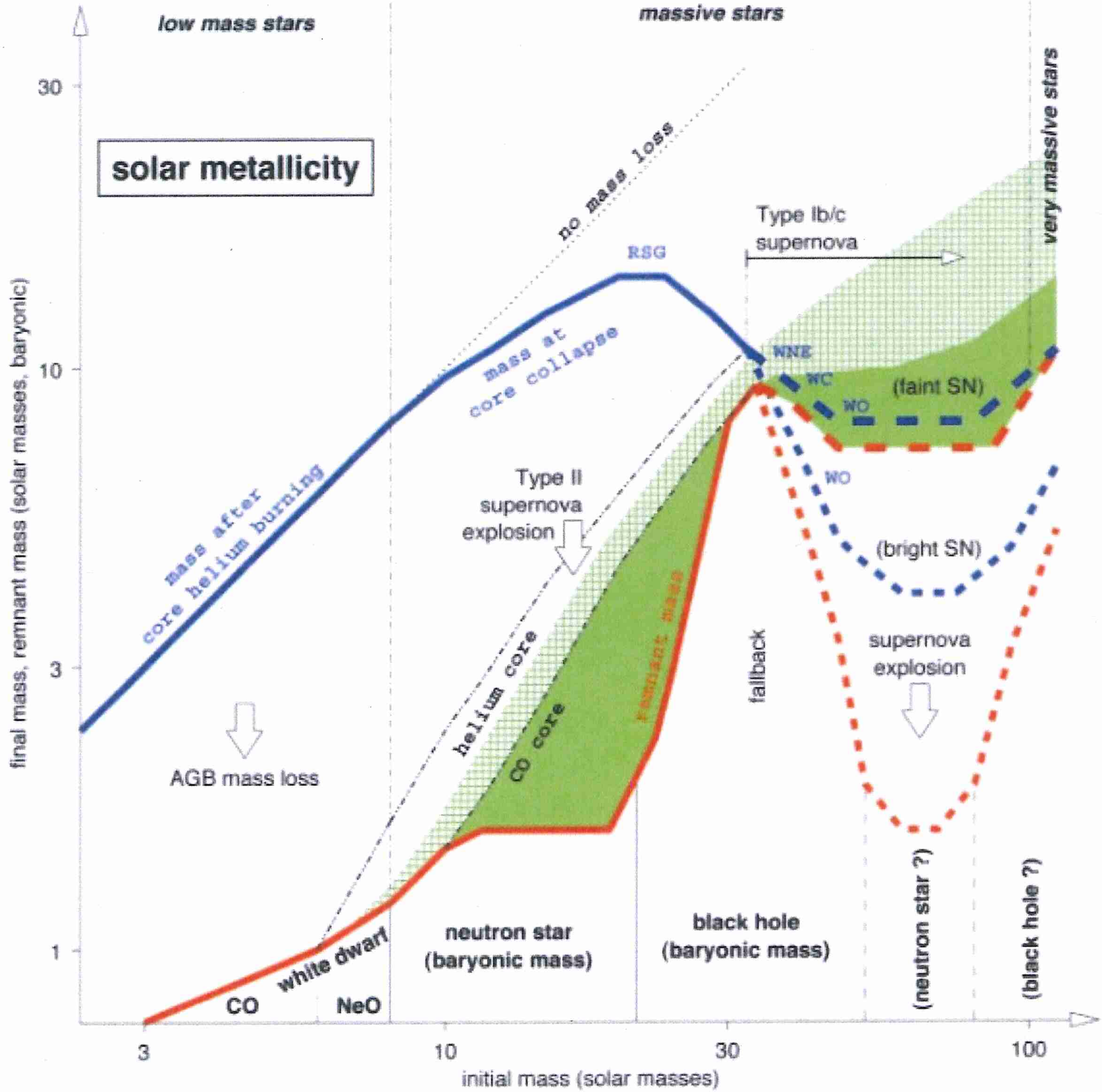

low mass stars
massive stars
very massive stars
solar metallicity
no mass loss
RSG
mass after core helium burning
mass at core collapse
Type Ib/c supernova
WNE
WC
WO
(faint SN)
WO
(bright SN)
Type II supernova explosion
helium core
CO core
remnant mass
fallback
supernova explosion
AGB mass loss
white dwarf
CO
NeO
neutron star (baryonic mass)
black hole (baryonic mass)
(neutron star ?)
(black hole ?)
final mass, remnant mass (solar masses, baryonic)
initial mass (solar masses)
30
10
3
1
3
10
30
100

FIG. 12. Initial-final mass function of nonrotating primordial stars ($Z=0$). The x axis gives the initial stellar mass. The y axis gives both the final mass of the collapsed remnant (thick red curve) and the mass of the star when the event that produces that remnant begins [e.g., mass loss in asymptotic giant branch (AGB) stars, supernova explosion for those stars that make a neutron star, etc.; thick blue curve]. Dark green indicates regions of heavy-element ($Z>2$) synthesis and cross-hatched green shows regions of partial helium burning to carbon and oxygen. We distinguish four regimes of initial mass: *low-mass stars* below $\sim 10M_{\odot}$ that form white dwarfs; *massive stars* between $\sim 10M_{\odot}$ and $\sim 100M_{\odot}$; *very massive stars* between $\sim 100M_{\odot}$ and $\sim 1000M_{\odot}$; and *supermassive stars* (arbitrarily) above $\sim 1000M_{\odot}$. Since no mass loss is expected for $Z=0$ stars, the blue curve corresponds approximately to the (dotted) line of no mass loss, except for $\sim 100-140M_{\odot}$ where the pulsational pair instability ejects the outer layers of the star before it collapses, and above $\sim 500M_{\odot}$ where pulsational instabilities in red supergiants may lead to significant mass loss. Since the magnitude of the latter is uncertain, lines are dashed. In the low-mass regime we assume, even in $Z=0$ stars, that mass loss on the asymptotic giant branch removes the envelope of the star, leaving a CO or NeO white dwarf (though the mechanism and thus the resulting initial-final mass function may differ from solar composition stars). Massive stars are defined as stars that ignite carbon and oxygen burning nondegenerately and do not leave white dwarfs. The hydrogen-rich envelope and parts of the helium core (dash-double-dotted curve) are ejected in a supernova explosion. Below initial masses of $\sim 25M_{\odot}$ neutron stars are formed. Above that, black holes form, either in a delayed manner by fallback of the ejecta or directly during iron-core collapse (above $\sim 40M_{\odot}$). The defining characteristic of very massive stars is their electron-positron pair instability after carbon burning. This begins as a pulsational instability for helium cores of $\sim 40M_{\odot}$ ($M_{\mathrm{ZAMS}} \sim 100M_{\odot}$). As the mass increases, the pulsations become more violent, ejecting any remaining hydrogen envelope and an increasing fraction of the helium core itself. An iron core can still form in hydrostatic equilibrium in such stars, but it collapses to a black hole. Above $M_{\mathrm{He}}=63M_{\odot}$ or about $M_{\mathrm{ZAMS}}=140M_{\odot}$, and on up to $M_{\mathrm{He}}=133M_{\odot}$ or about $M_{\mathrm{ZAMS}}=260M_{\odot}$, a single pulse disrupts the star. Above $260M_{\odot}$, the pair instability in nonrotating stars results in complete collapse to a black hole [Color].

TO CORE COLLAPSE

- H, He, C, Ne, O, Si : HYDROSTATIC BURNING : ONION SKIN (?)
- WEAK s-PROCESS
  - He-CORE BURNING
    $^{22}Ne(\alpha,n)^{25}Mg$ $T \sim 3 \times 10^8 K$
  - C-SHELL BURNING
    $^{22}Ne(\alpha,n)^{25}Mg$
    $^{12}C(^{12}C,\alpha)^{20}Ne$

→ FEW NEUTRONS → LITTLE Fe-GROUP CONVERSION TO Zn to Zr PRODUTION

→ PRODUTION depends on rate for $^{22}Ne(\alpha,n)$ vs. $^{22}Ne(\alpha,\gamma)$

END OF Si-BURNING → CORE COLLAPSE

- ^{56}Fe = NO NUCLEAR ENERGY SOURCE
  BUT MASS ↑ VIA Si-SHELL BURNING
- CORE $> 1.4 M_\odot$ → COLLAPSE
  AT c/4
  - → DENSITY TO NUCLEAR DENSITY (10^{14} g/cm^3)
  - → SHORT-RANGE REPULSIVE NUCLEAR FORCE → COLLAPSE HALT + BOUNCE
  - → SHOCK GOES OUT FROM CORE
  - → SHOCK MEETS INFALLING MASS, LOSE ENERGY (PHOTODIS. OF Fe, ν EMISSION)

→ SHOCK STALLS IN 'ALL' CALCULATIONS (ADD D's?)

EXPLOSION MECHANISM STILL BEING SOUGHT !

∴ IMPOSE AN ARTIFICIAL STIMULANT

- ADD ENERGY or PISTON
- SELECT MASS OUT

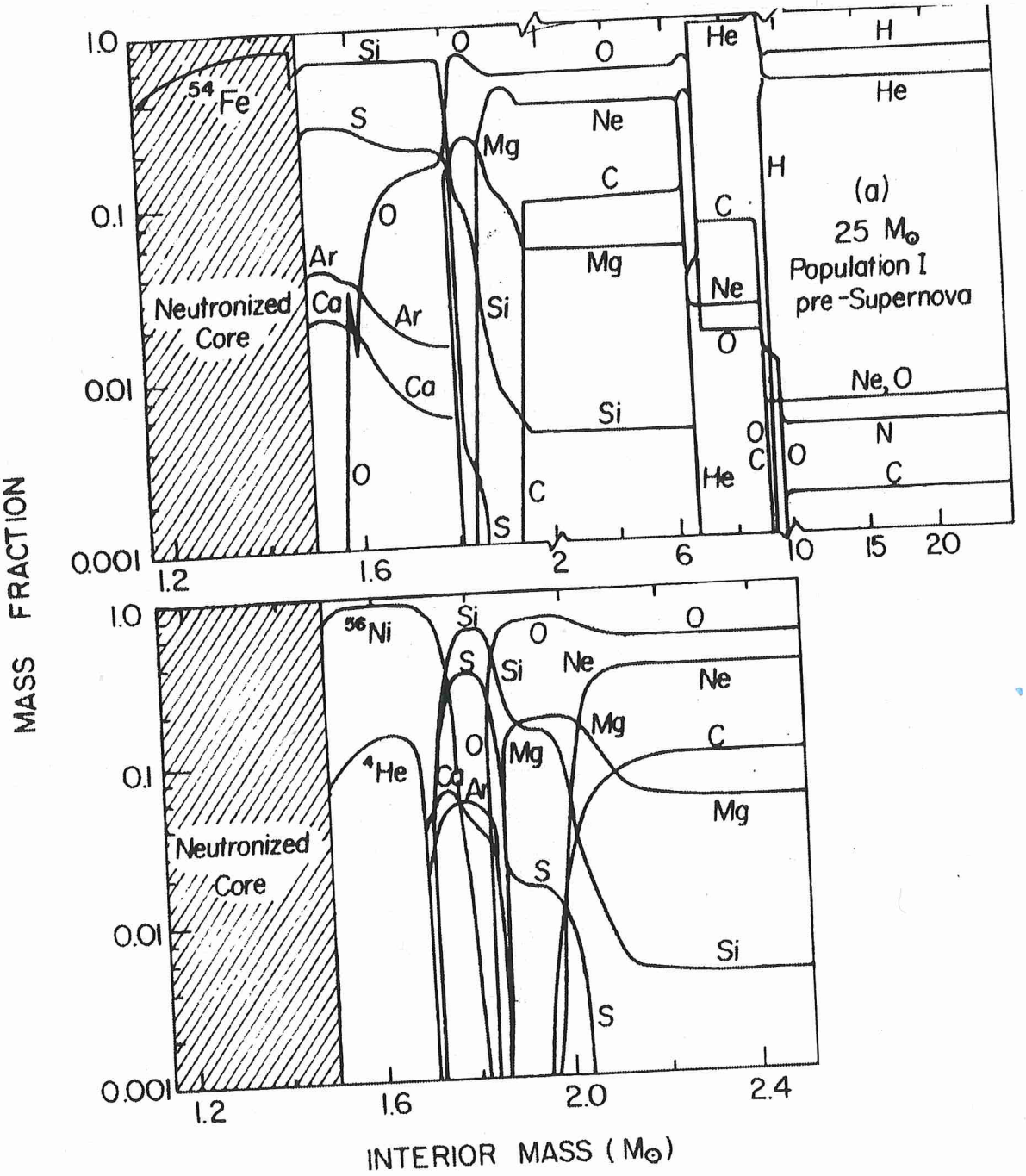

Fig. 5.10. Upper panel: chemical profile of a 25 $M_\odot$ star immediately before core collapse. (Note change in horizontal scale at 2 $M_\odot$.) Lower panel: the same, after modification by explosive nucleosynthesis in a supernova outburst. The amount of ^{56}Ni (which later decays to ^{56}Fe) ejected depends on the mass cut, somewhere in the ^{28}Si$\rightarrow$^{56}Ni zone, and is uncertain by a factor of 2 or so. Adapted from Woosley and Weaver (1982).

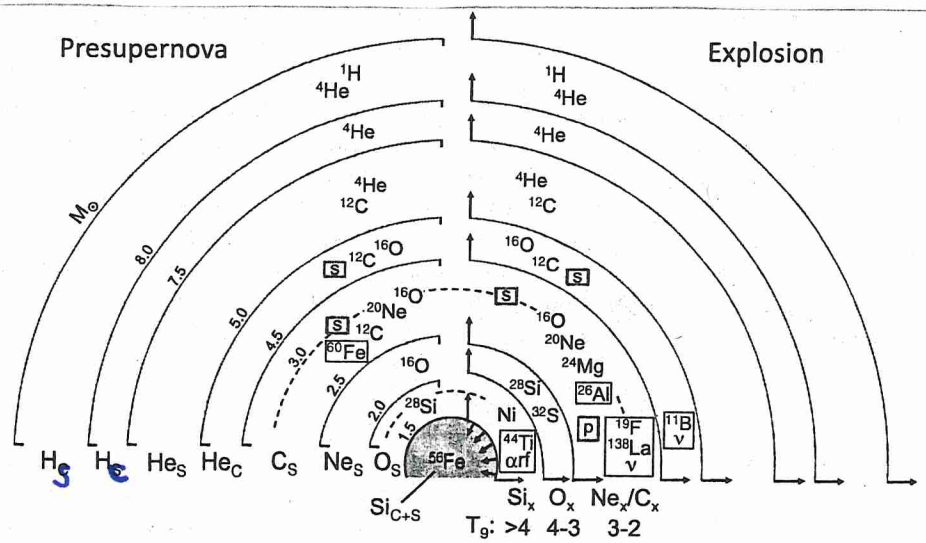

Figure 6. Structure and evolution of a $25M_{\odot}$ star of solar metallicity, as predicted by one-dimensional, spherically symmetric models [91, 132], shortly before and after core-collapse (not to scale). Only the main constituents in each layer are shown. Minor constituents, among them important γ-ray emitters, are set in thin black boxes. Various nucleosynthesis processes are shown in green boxes: weak s-process (s); p-process (p); α-rich freeze-out (αrf); ν-process (ν). Left: snapshot of pre-supernova structure. Nuclear burning takes place in thin regions (burning shells) at the interface of different compositional layers, where each burning shell migrated outward to the position indicated by the blue lines. The compositions result from burning stages indicated at the bottom (subscripts C and S stand for core and shell burning, respectively). The diagonally arranged numbers indicate the interior mass (in solar masses) for each burning shell. Right: Explosive nucleosynthesis resulting from passage of the shock wave through overlying layers, giving rise to explosive burning of silicon (Si_x), oxygen (O_x) and neon–carbon (Ne_x/C_x). Strictly speaking, this classification depends on the temperature range, not on the available fuel. Nevertheless, the names indicate approximately which compositional layers of the pre-supernova will usually be affected. Outside the outer dashed line, the composition is little altered by the shock. The inner dashed line indicates the approximate boundary of the part of the star that is ejected (mass cut).

MAJOR UNCERTAINTIES AFFECTING PRE-SN II STRUCTURE

- NUCLEAR PHYSICS
  - $^{12}C(\alpha,\gamma)^{16}O$ STILL?
  - ?
- MASS LOSS
  - → WOLF-RAYET STARS
    - WN, WC, WO
    - SN Ib-Ic
- CONVECTION
- ROTATION (mixing, asymmetry)
- MAGNETIC FIELD

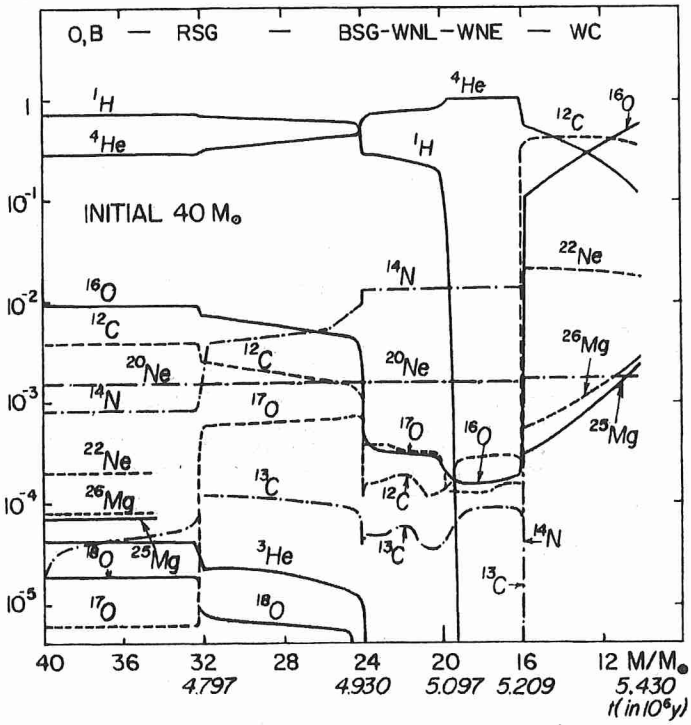

Fig. 5.13. Time evolution of the chemical profile of a 40 $M_\odot$ star that becomes a Wolf–Rayet star as a result of the outer layers peeling off in stellar winds. The spectrum evolves from type O to type B to a red supergiant (RSG) and then back to a blue supergiant (BSG) and towards increasing effective temperatures ending up well to the left of the main sequence. The chemically modified spectrum evolves from nitrogen-rich late, i.e. relatively cool (WNL), to nitrogen-rich early (WNE) to carbon-rich (WC); in some cases still hotter stars are observed that are oxygen-rich (WO). After Maeder and Meynet (1987).

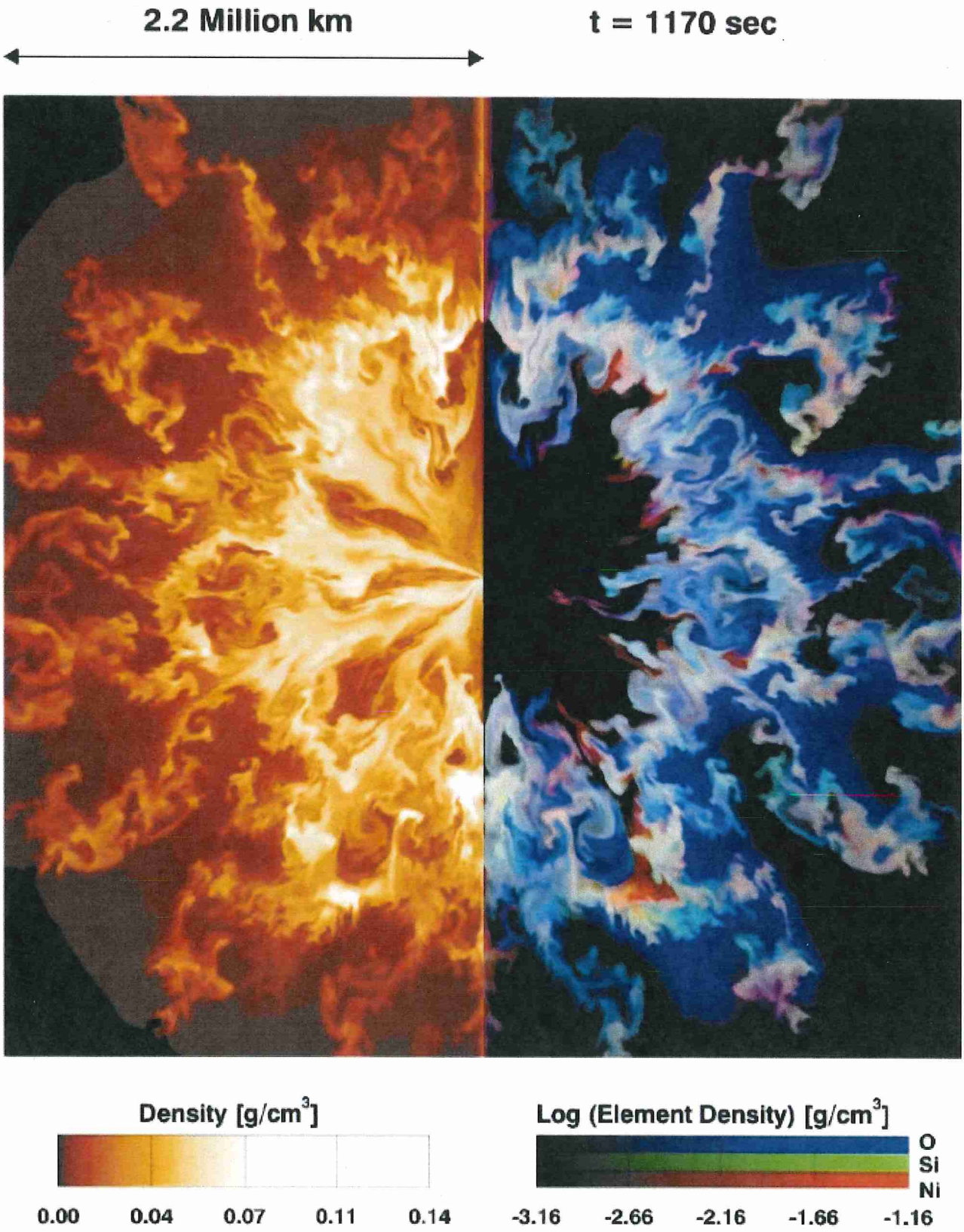

FIG. 24. Mixing in the explosion of a $15M_\odot$ red supergiant. From Kifonidis *et al.*, 2000 [Color].

they eject too much neutron-rich nucleosynthesis. Most of the calculations so far follow the explosion for a very limited time and it is not known with any accuracy how the kinetic energy produced by the supernova depends on the initial stellar mass (though see Fryer, 1999). Those calculations that do produce an explosion tend to blow away a portion of the neutron star and leave remnant masses that are too small. The degree of fallback

N' SYNTHESIS AT EXPLOSION

- EXPLOSIVE N' SYNTHESIS
- r- PROCESS
- ν - PROCESS
- p - PROCESS
- νp - PROCESS

EXPLOSIVE NUCLEOSYNTHESIS

- 1970+'s

  SUMMARY: CLAYTON + WOOSLEY
  Rev. Mod Phys. 46 755 1974

- EXPANSION TIMESCALE

$$\tau_{ff} = \frac{1}{\sqrt{24\pi G \rho_0}} = \frac{446}{\sqrt{\rho_0}} \quad [s]$$

$$\tau_{exp} = \chi \tau_{ff} \qquad (\chi \sim 1)$$

$$\rho(t) = \rho_0 \exp\left(-\frac{t}{t_{exp}}\right) \qquad [g/cm^3]$$

$$\rho \propto T^3 \quad \text{(adiabatic)}$$

- H, He, C, Ne, O, Si STUDIED

EXPLOSIVE Si-BURNING

- INCOMPLETE Si-BURNING AND COMPLETE Si-BURNING WITH EITHER A NORMAL OR AN α-RICH FREEZE OUT

AT HIGH T & ρ
→ NSE & STAY IN NSE AS T COOLS QUICKLY

^{56}Ni

AT [redacted] HIGH T & LOWER ρ
→ α-RICH FREEZE OUT
(3α → ^{12}C; ^{4}He(αn,γ)^{9}Be)
too slow to keep n, p, α in NSE

AT 'LOW' T → INCOMPLETE Si-BURN.
O, NeC, GLS

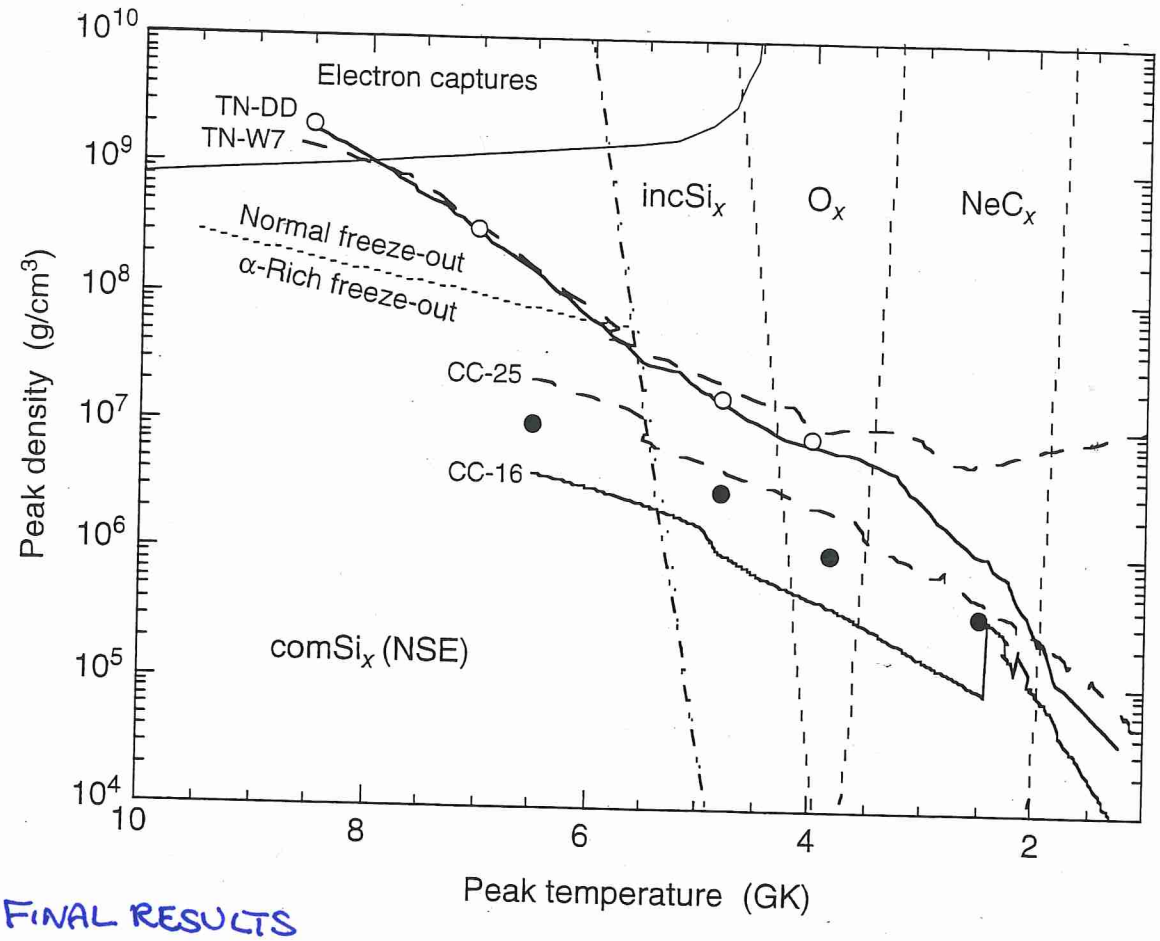

FINAL RESULTS

Figure 5.42 Peak temperatures and peak densities attained in different mass zones during the outward propagation of burning fronts in supernova explosion models. The two lower tracks are from core-collapse (type II, Ib, Ic) supernova models (CC-16: Young *et al.*, 2006; CC-25: Limongi and Chieffi, 2003), while the two upper tracks are from thermonuclear (type Ia) supernova models (TN-W7: Nomoto, Thielemann, and Yokoi, 1984; TN-DD: Bravo and Martínez-Pinedo, 2012). Regions of predominant nucleosynthesis processes are indicated: complete silicon burning ("comSi$_x$ (NSE)", entire region to the left of dashed-dotted line); normal freeze-out (above dotted line); α-rich freeze-out (below dotted line); incomplete silicon burning ("incSi$_x$"), explosive oxygen burning ("O$_x$"), and explosive neon-carbon burning ("NeC$_x$"). The boundaries between the different regions depend on the explosion time scale and are only approximate. The gray shaded area at the top left indicates the region where electron captures change the neutron excess significantly during the explosion (Section 5.5.1). The full and open circles mark peak temperature and density conditions adopted for the reaction network calculations discussed in the text.

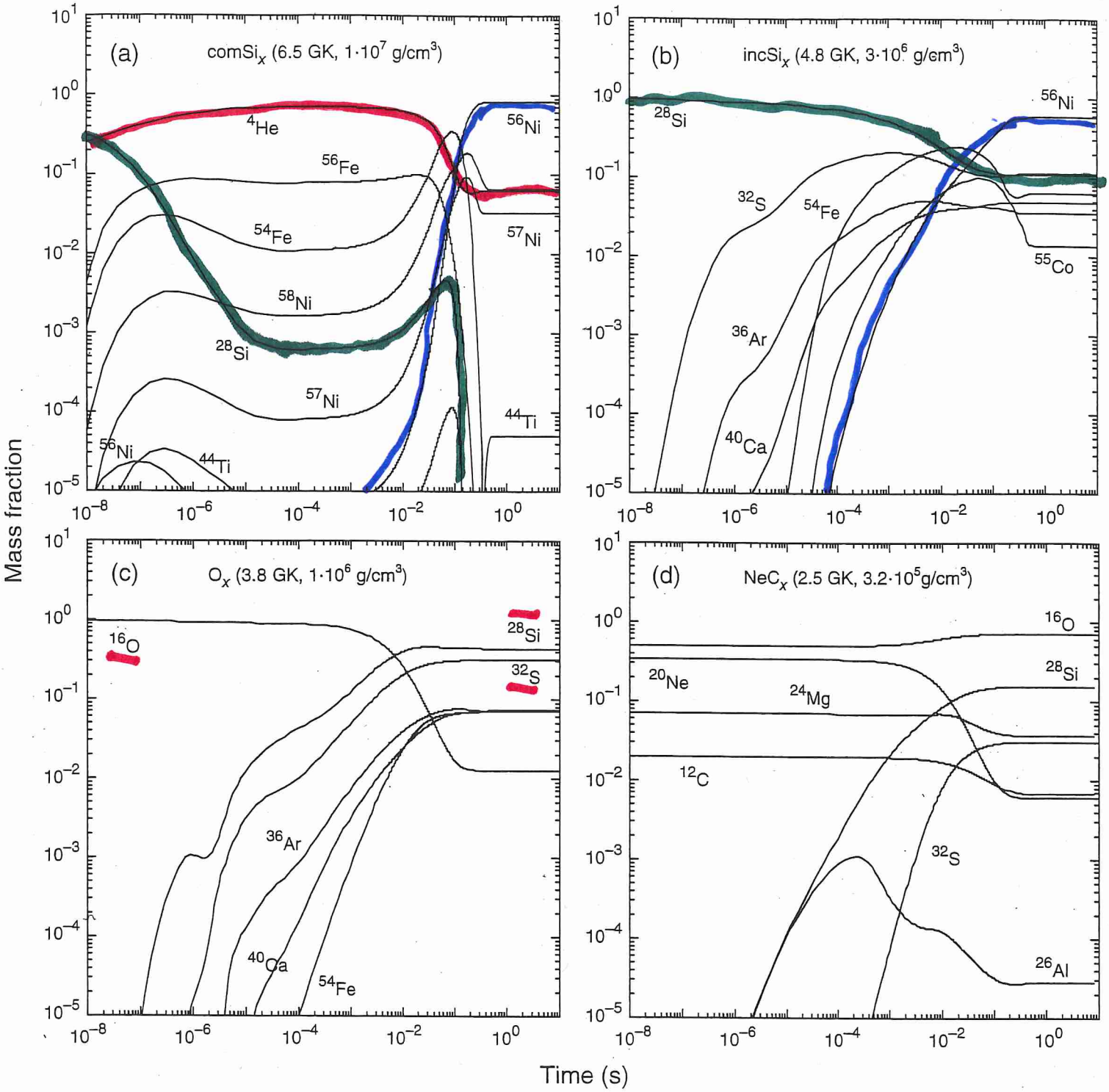

Figure 5.44 Abundance evolutions for explosive nucleosynthesis in core collapse supernovae (type II, Ib, Ic). Results are obtained using exponential T-ρ trajectories (see Eqs. (5.145) and (5.144)) that approximate the conditions in the outward moving shock. Adopted values of T_{peak}, ρ_{peak}, τ_{hd} are: (a) 6.5 GK, 10^7 g/cm^3, 0.14 s; (b) 4.8 GK, 3×10^6 g/cm^3, 0.26 s; (c) 3.8 GK, 10^6 g/cm^3, 0.45 s; (d) 2.5 GK, 3.2×10^5 g/cm^3, 0.79 s. These conditions correspond to complete explosive silicon burning, incomplete explosive silicon burning, explosive oxygen burning, and explosive neon-carbon burning, respectively, and are marked by solid circles in Figure 5.42. All results shown are obtained with an initial neutron excess of $\eta = 0.003$.

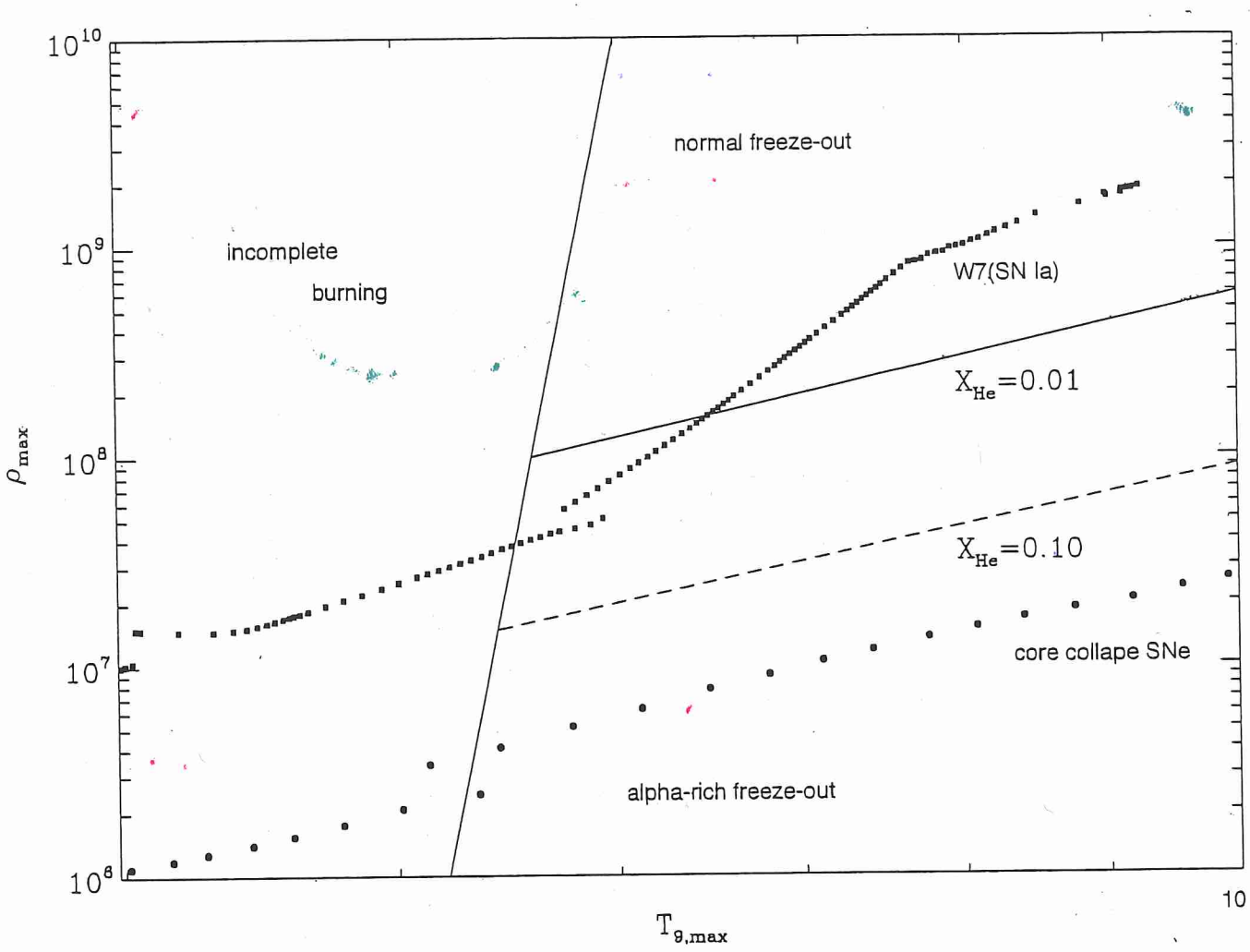

Fig. 4.2 Final results of explosive Si-burning as a function of maximum temperatures and densities attained in explosions before adiabatic expansion. For temperatures in excess of 5×10^9K any fuel previously existing is photodisintegrated into nucleons and α particles before re-assembling in the expansion. For high densities this is described by a full NSE with an Fe-group composition, favoring nuclei with maximum binding energies and proton/nucleon ratios equal to Y_e. For lower densities the NSE breaks into local equilibrium groups (quasi-equilibrium, QSE) with group boundaries determined by reactions with an insufficiently fast reaction stream. Alpha-rich freeze-out (insufficient conversion of α particles into nuclei beyond carbon) is such a QSE-behavior. Lines with 1% and 10% remaining α-particle mass fraction are indicated as well as typical conditions for mass zones in type Ia and core-collapse supernovae.

4.2 – 4.14 from Thielemann et al.
Massive stars & their supernovae
Astronomy with Radioactivities
Springer 2011

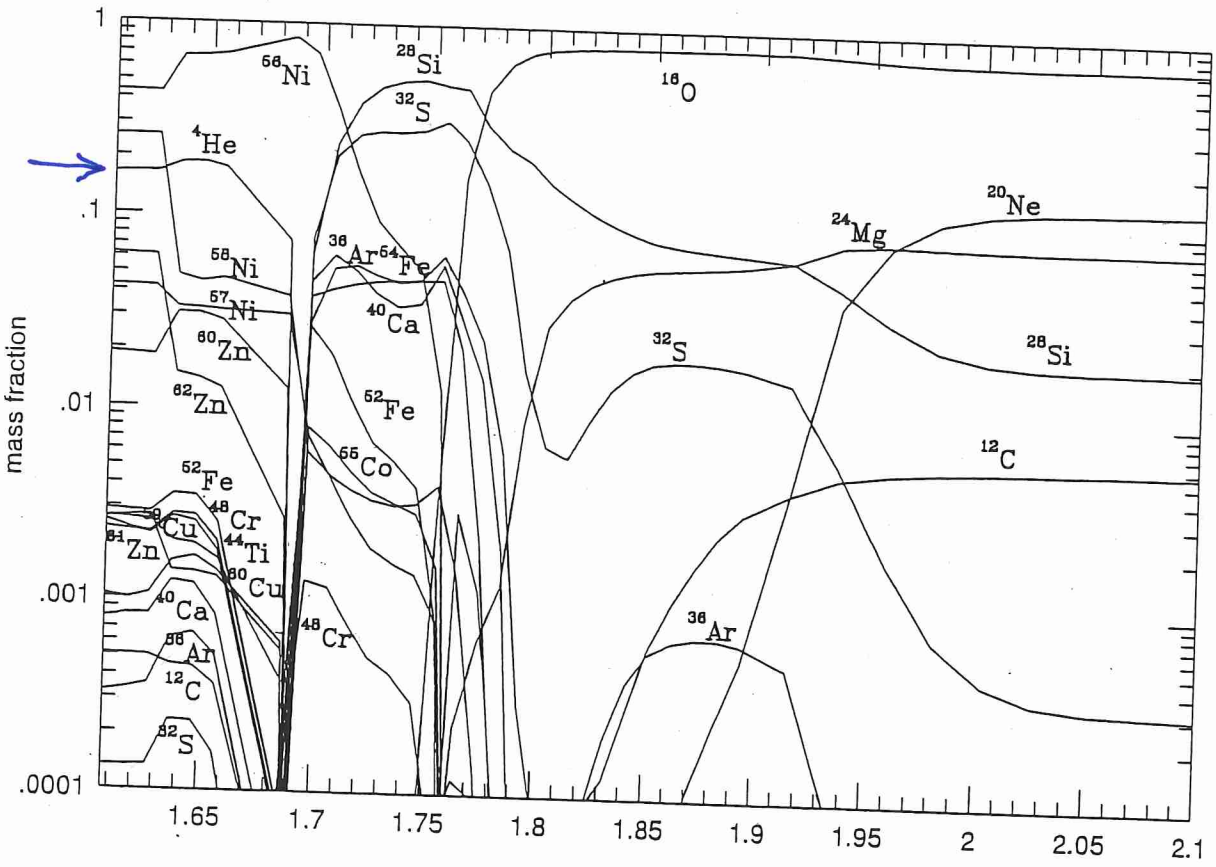

Fig. 4.11 Mass fractions of a few major nuclei after passage of the supernova shockfront through a star with an intial mass of 20 $M_\odot$. Matter outside $2M_\odot$ is essentially unaltered. Mass zones further in experience explosive Si, O, Ne, and C-burning. For ejecting $0.07M_\odot$ of ^{56}Ni the mass cut between neutron star and ejecta is required to be located at $1.6M_\odot$.

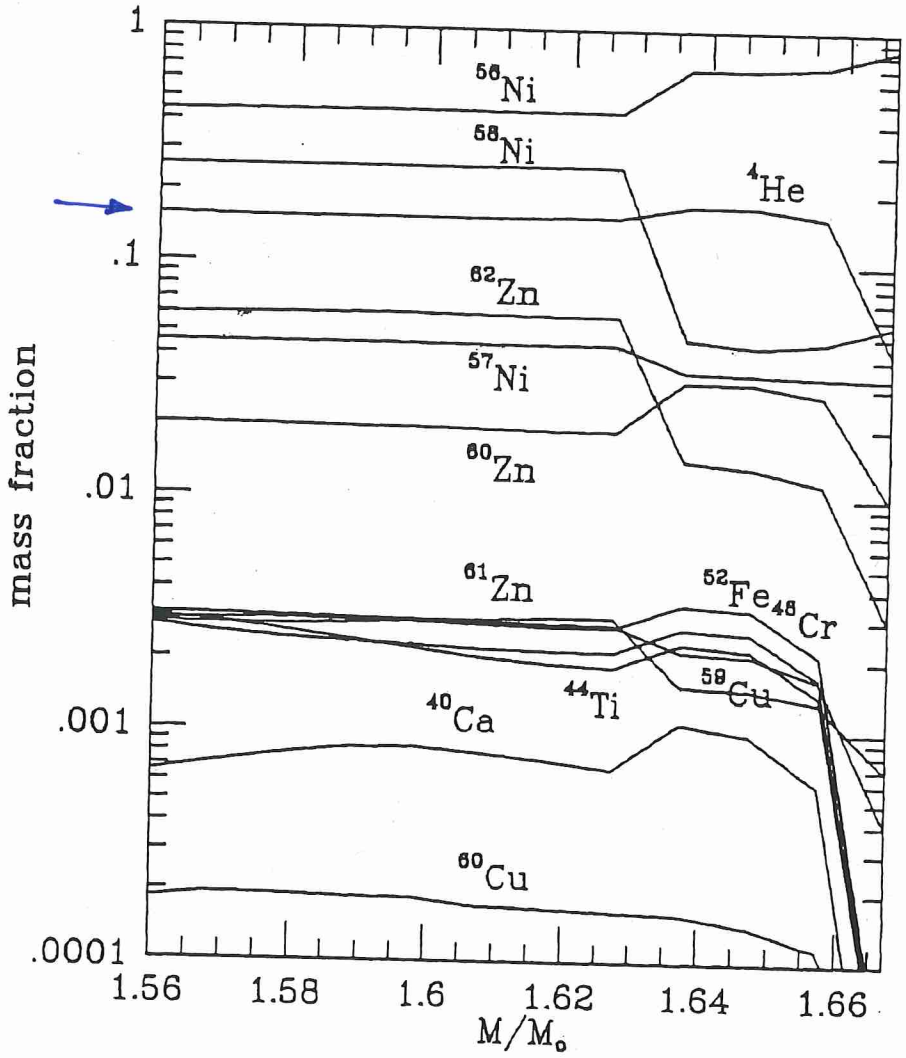

Fig. 4.12 Mass fractions of the dominant nuclei in zones which experience α-rich freeze-out. Notice the relatively large amounts of Zn and Cu nuclei, which originate from α-captures on Ni and Co. One can recognize their strong decrease beyond $1.66M_{\odot}$, which goes parallel with the decrease of the ^{4}He-abundance and other α-nuclei such as ^{40}Ca, ^{44}Ti, ^{48}Cr, and ^{52}Fe. Nuclei which would dominate in a nuclear statistical equilibrium like ^{56,57,58}Ni stay constant or increase even slightly. The increase of all nuclei with $N = Z$ at $1.63M_{\odot}$ and the decrease of nuclei with N>Z is due to the change in Y_e in the original stellar model before collapse (see also Fig.4.11)

expansion of Fig 4.11

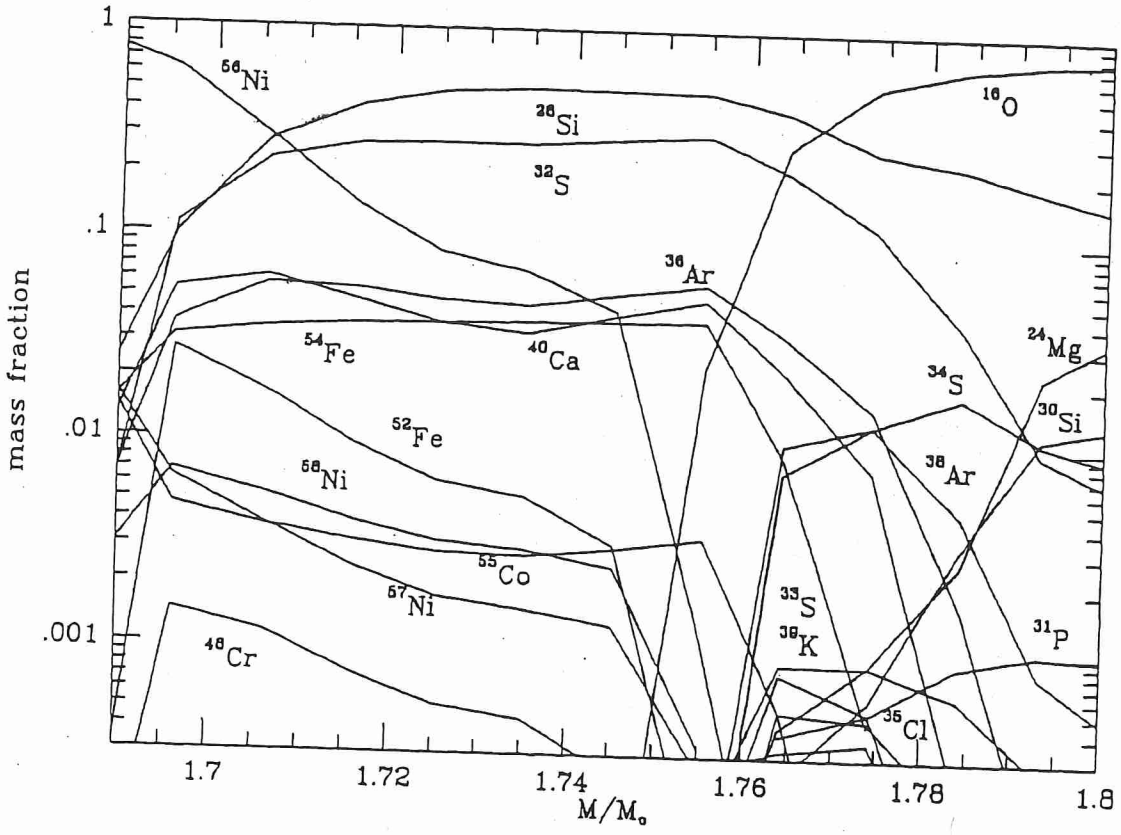

Fig. 4.13 Mass fractions of nuclei in the zones of incomplete Si-burning $M<1.74M_\odot$ and explosive O-burning $M<1.8M_\odot$. The Si-burning zones are are characterized by important quantities of Fe-group nuclei besides ^{28}Si, ^{32}S, ^{36}Ar, and ^{40}Ca. Explosive O-burning produces mostly the latter, together with more neutron-rich nuclei like ^{30}Si, ^{34}S, ^{38}Ar etc.

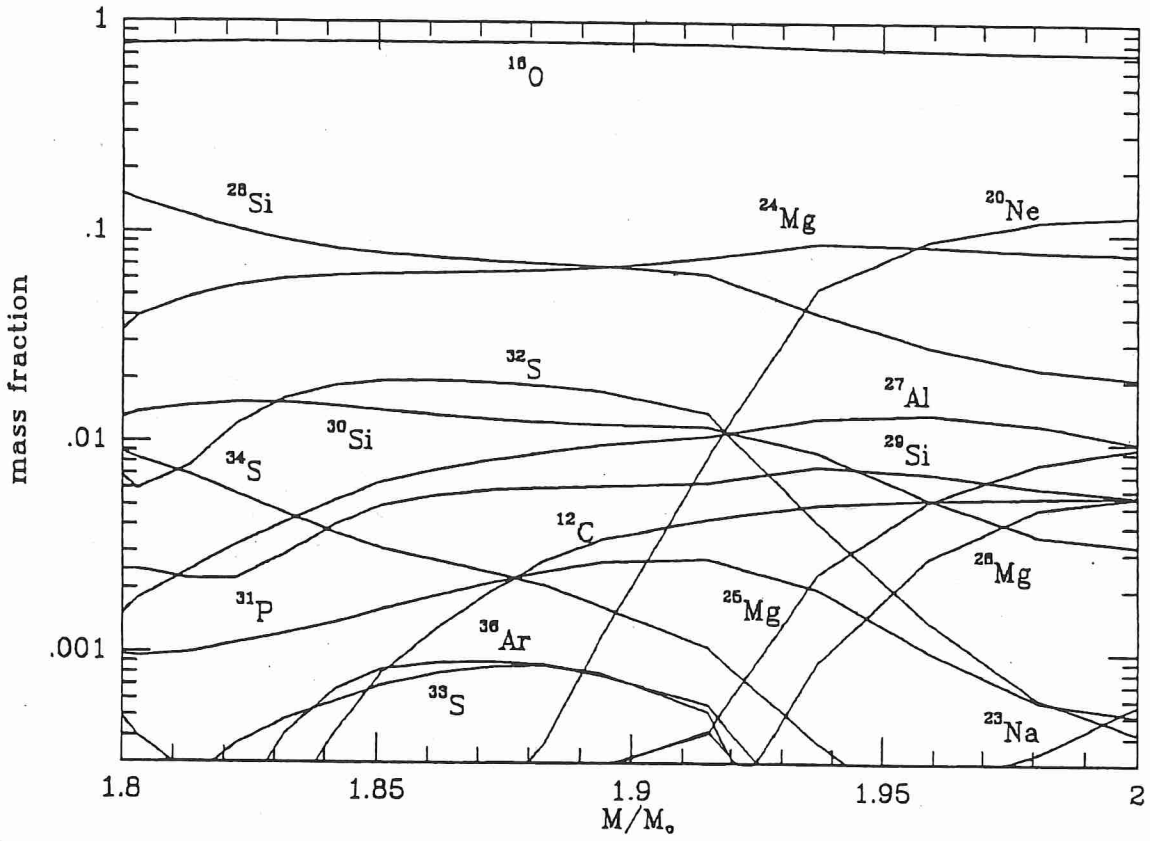

Fig. 4.14 Composition in mass zones of explosive Ne and C-burning. The dominant products are ^{16}O, ^{24}Mg, and ^{28}Si. Besides the major abundances, mentioned above, explosive Ne-burning supplies also substantial amounts of ^{27}Al, ^{29}Si, ^{32}S, ^{30}Si, and ^{31}P. Explosive C-burning contributes in addition the nuclei ^{20}Ne, ^{23}Na, ^{24}Mg, ^{25}Mg, and ^{26}Mg.

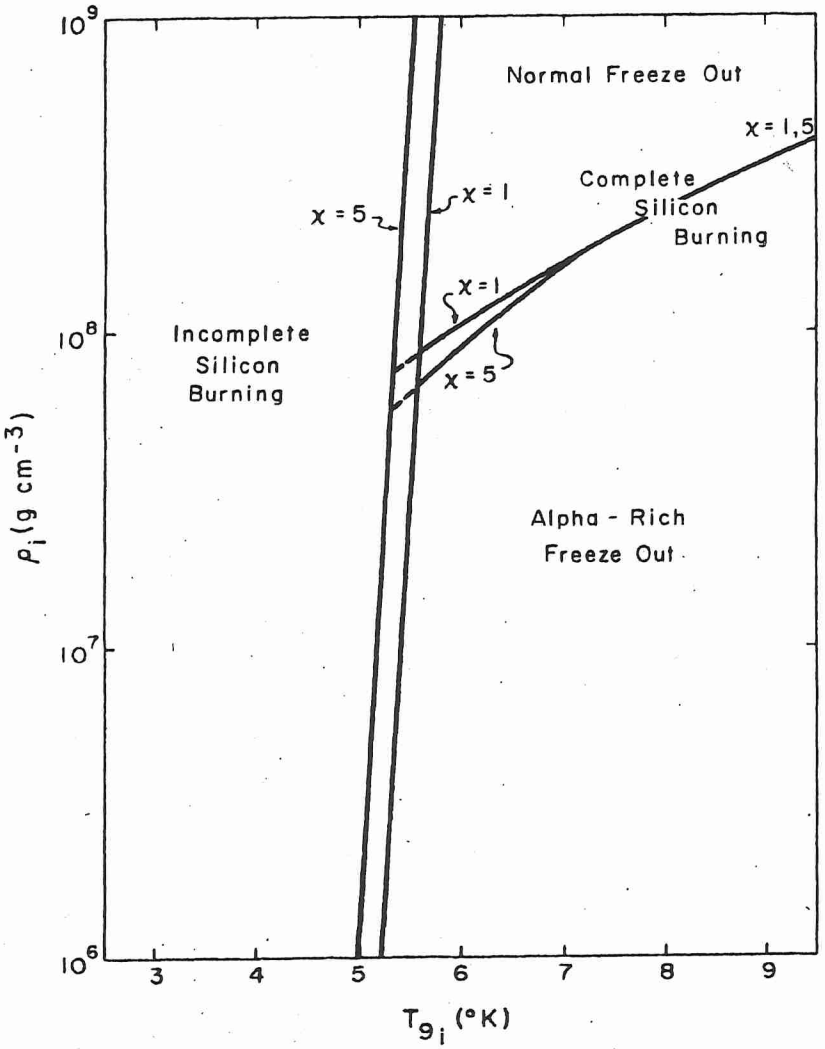

FIG. 10. Final state of explosions from differing initial temperatures (T_{9i}) and densities (ρ_i). For $T_{9i} < 5$, ^{28}Si is not completely burned and quasiequilibrium with ^{28}Si exists in the ejecta. For $T_{9i} > 5.5$, nuclear equilibrium is established and has a normal freeze-out at high initial density; however, for $\rho_i < 10^8$ gm cm^{-3}, excess free particles remain as the nuclear equilibrium expands and cools. Final abundances differ markedly for ejecta from these three differing types of explosions (Woosley, Arnett, and Clayton, 1973). The use of two time-scale parameters χ shows that the expansion rate has only a weak influence on this result.

EXPLOSIVE O

$T_9 \sim 3-4$

^{16}O dissociates

EXPLOSIVE C

$T_9 \sim 2-3$

^{28}Si ↑

SN II s & SOLAR ABUNDANCES

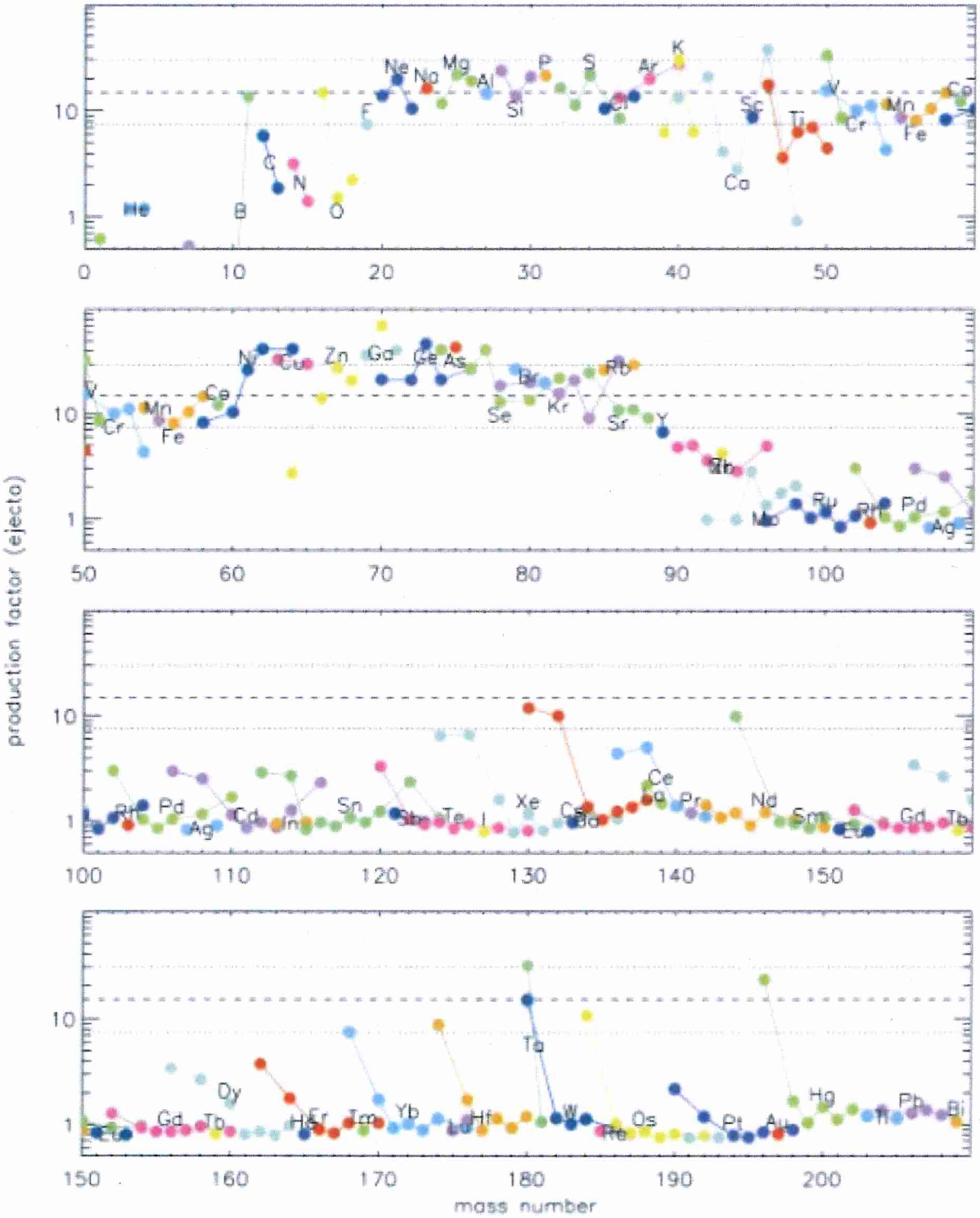

FIG. 27. Final nucleosynthesis from a $25M_{\odot}$ supernova compared to solar abundances (Heger, Woosley, Rauscher, and Hoffman, 2002). Isotopes of a given element are all the same color and are connected by lines. All ejecta, including the wind, are included. A possible *r* process in the neutrino wind is not taken into account here. The production factor is the ratio of the mass fraction in the ejecta divided by the mass fraction in the sun [Color].

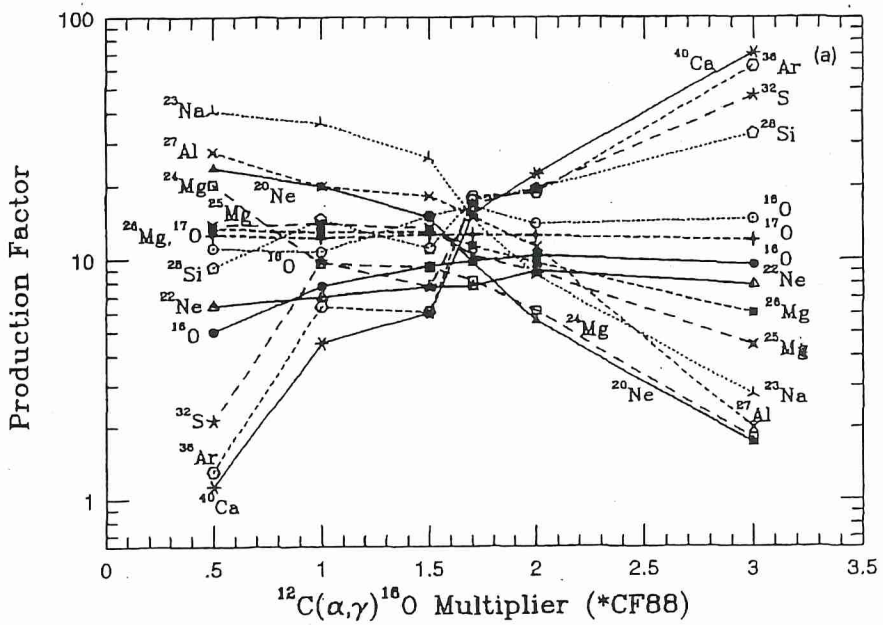

Fig. 6.5. Yields of nuclides relative to solar abundance as a function of the $^{12}C(\alpha,\gamma)^{16}O$ reaction cross section. As can be seen, the abundances of the nuclides vary wildly with this reaction rate, but remarkably all seem to fall into about the same production factor with a single value of the cross section. From Weaver and Woosley (1993). Copyright 1993, with permission from Elsevier.

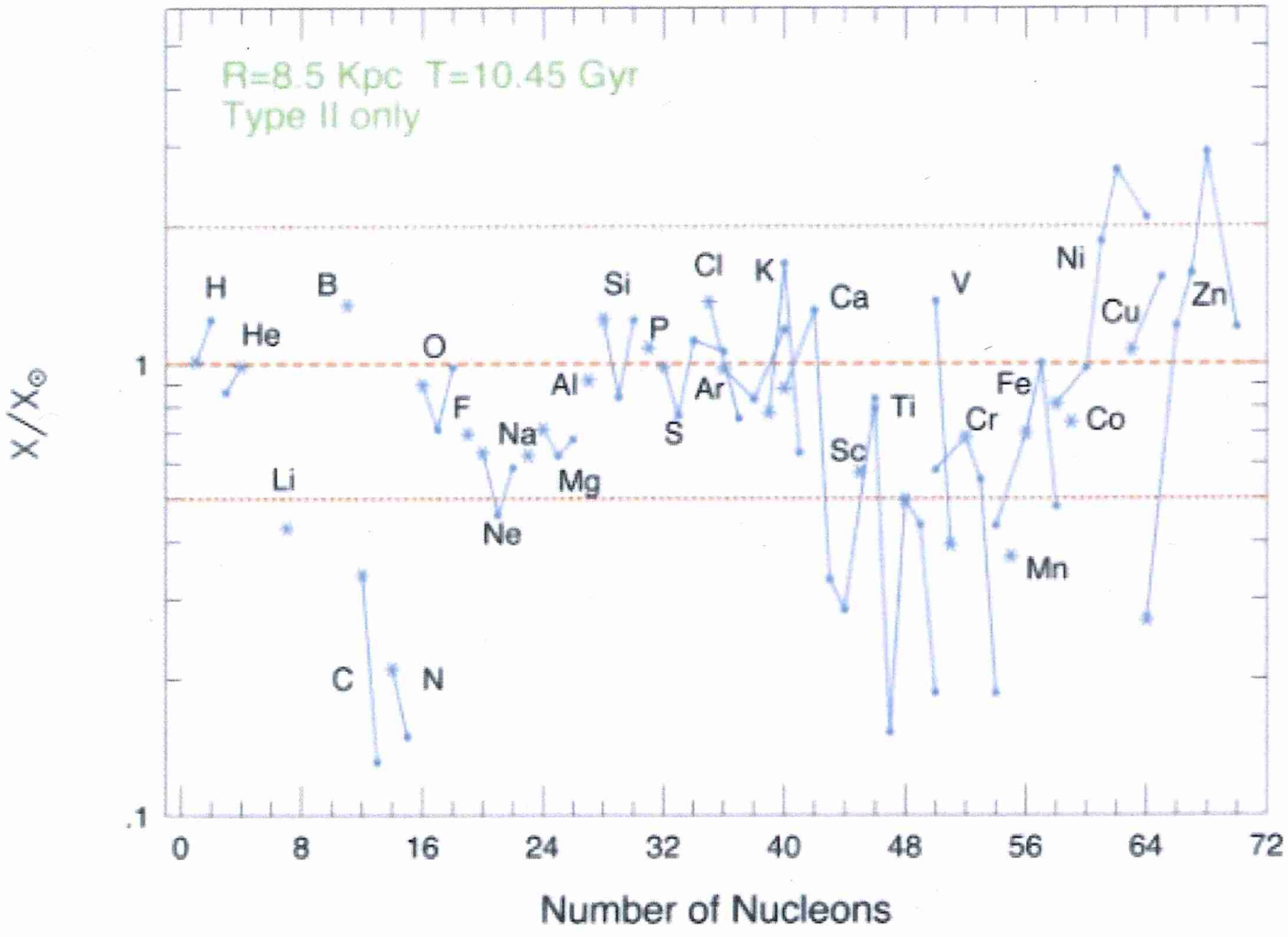

FIG. 28. Integrated nucleosynthesis from a grid of massive stars ($11-40M_{\odot}$) of various metallicities ($0Z_{\odot}$, $10^{-4}Z_{\odot}$, $0.01Z_{\odot}$, $0.1Z_{\odot}$, and $1Z_{\odot}$) compared to the solar abundances (Timmes, 1996). This figure also includes contributions from the big bang (hence ^{2}H) but not from low-mass stars (especially ^{12}C and ^{14}N) or type-Ia supernovae (especially ^{55}Mn, ^{54,56}Fe, and ^{58}Ni) or novae (^{15}N, ^{17}O). The overproduction of Zn and Ni isotopes may reflect an overly large rate for ^{22}Ne$(\alpha,n)^{25}$Mg during the *s* process [Color].

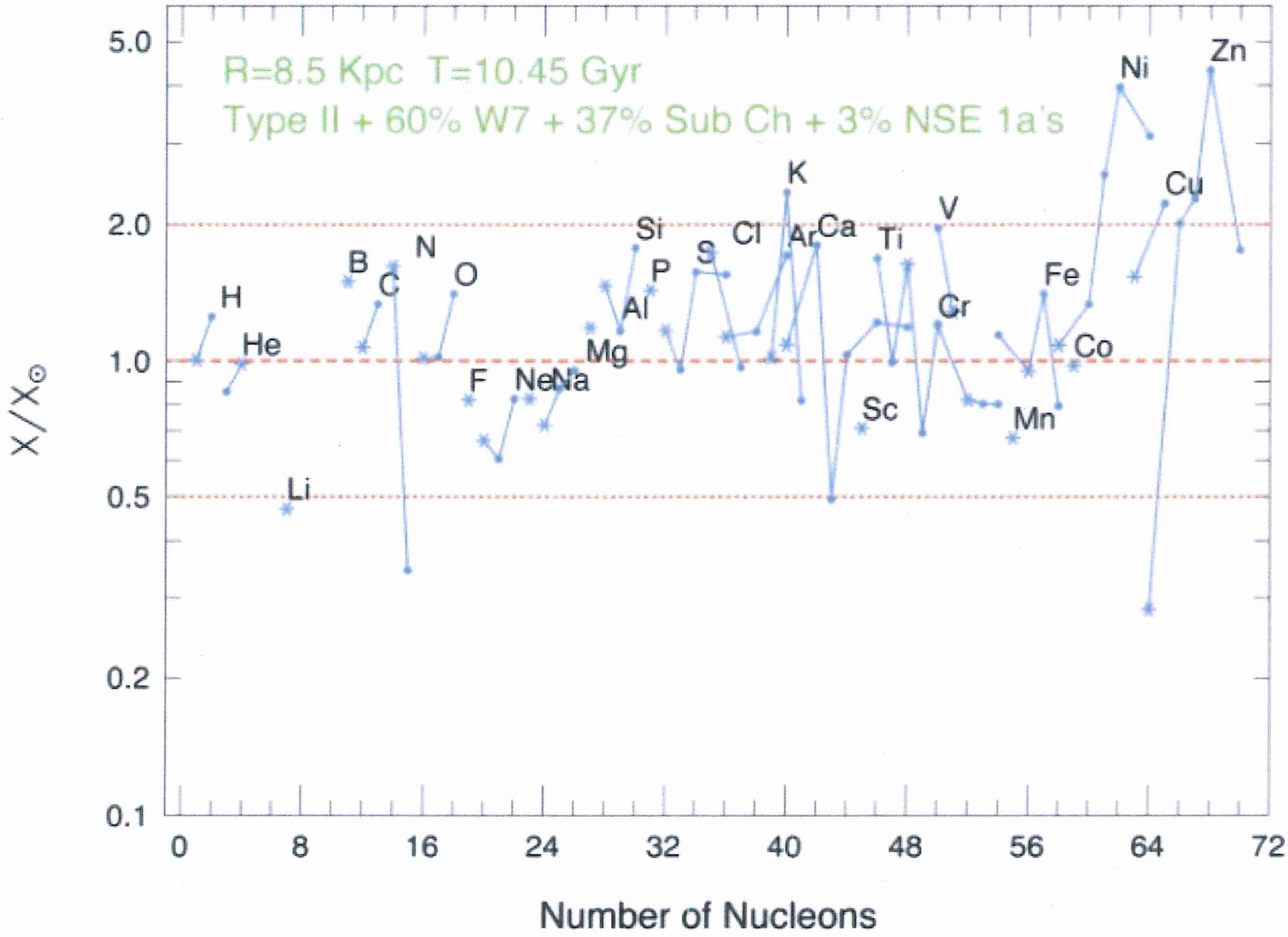

FIG. 29. The agreement in Fig. 28 is greatly improved if one includes the iron-group production from three varieties of type-Ia supernovae (see text and Table III) as well as classical novae (Timmes, 1996) [Color].

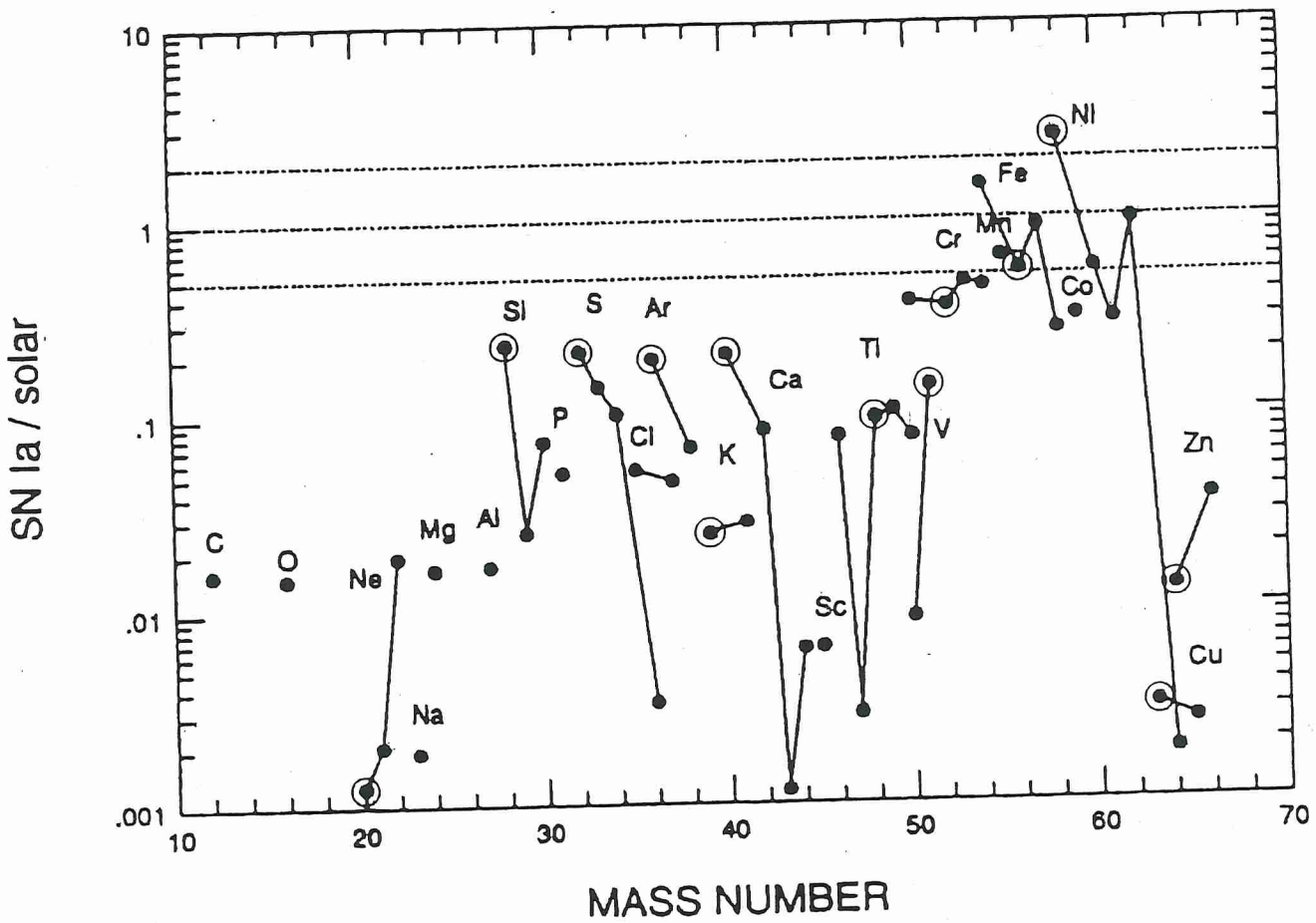

Fig. 5.25. Nucleosynthetic outcome (after radioactive decay) of model W7 for Type Ia supernovae (Nomoto, Thielemann & Yokoi 1984, and Thielemann, Nomoto & Yokoi 1986), compared to Solar-System abundances. Dominant isotopes of multi-isotope elements are circled. Adapted from Tsujimoto (1993).

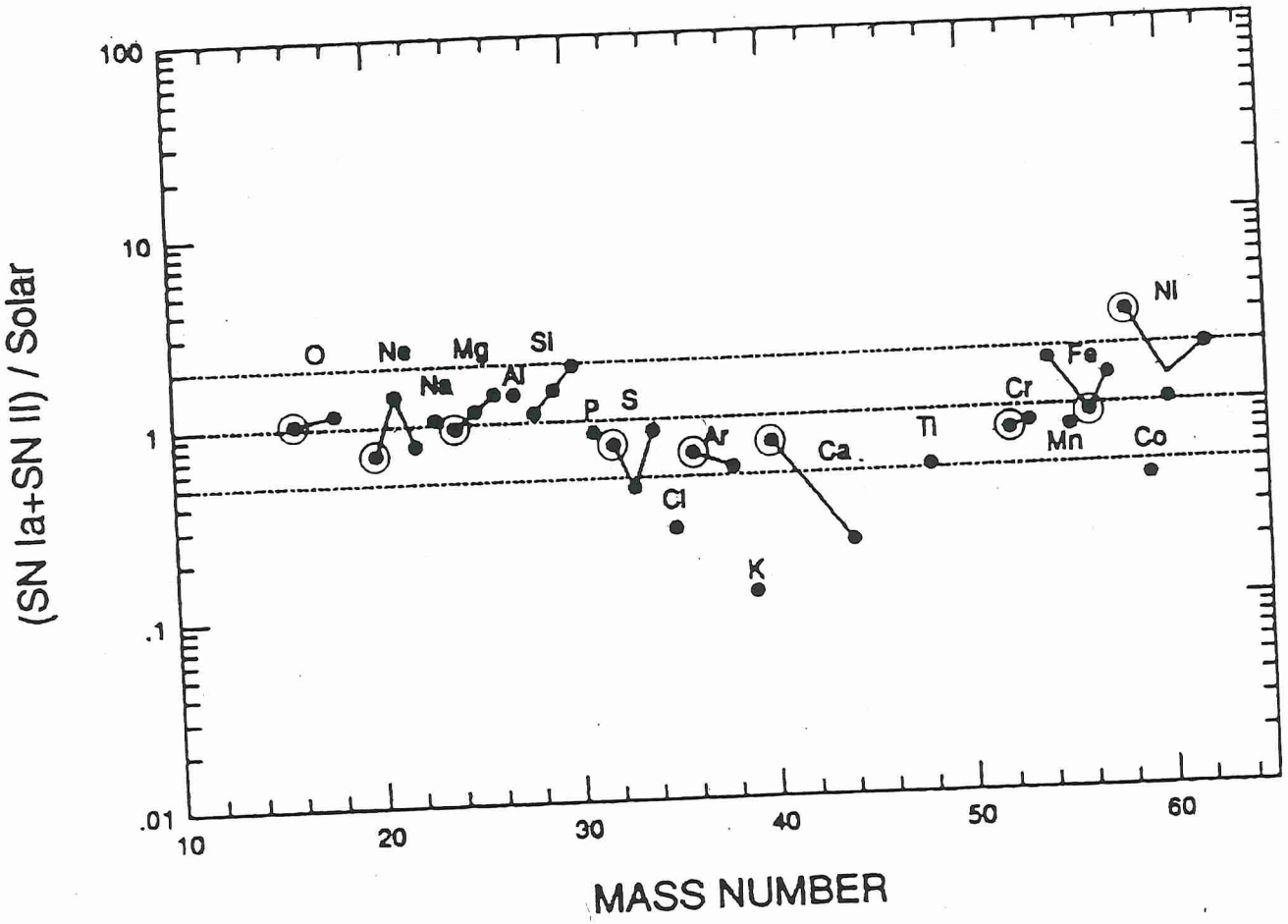

Fig. 5.26. Nucleosynthesis products from SN Ia (Fig. 5.25) and SN II (Fig. 5.12) combined in a ratio of 1:10, compared to Solar-System abundances. (A slightly higher ratio of 1:7 gives optimal fit to elemental, as opposed to individual nuclidic abundances.) Dominant isotopes of multi-isotope elements are circled. Adapted from Tsujimoto (1993).

TABLE III. The origin of the light and intermediate-mass elements.

Species	Origin	Species	Origin	Species	Origin
^{1}H	BB	^{30}Si	C,Ne	^{51}V	α,Ia-det,xSi,xO,ν
^{2}H	BB	^{31}P	C,Ne	^{50}Cr	xSi,xO,α,Ia-det
^{3}He	BB,L*	^{32}S	xO,O	^{52}Cr	xSi,α,Ia-det
^{4}He	BB,L*,H	^{33}S	xO,xNe	^{53}Cr	xO,xSi
^{6}Li	CR	^{34}S	xO,O	^{54}Cr	nse-IaMCh
^{7}Li	BB,ν,L*,CR	^{36}S	He(s),C,Ne	^{55}Mn	Ia,xSi,ν
^{9}Be	CR	^{35}Cl	xO,xNe,ν	^{54}Fe	Ia,xSi
^{10}B	CR	^{37}Cl	He(s),xO,xNe	^{56}Fe	xSi,Ia
^{11}B	ν	^{36}Ar	xO,O	^{57}Fe	xSi,Ia
^{12}C	L*,He	^{38}Ar	xO,O	^{58}Fe	He(s),nse-IaMCh
^{13}C	L*,H	^{40}Ar	He(s),C,Ne	^{59}Co	He(s),α,Ia,ν
^{14}N	L*,H	^{39}K	xO,O.ν	^{58}Ni	α
^{15}N	novae,ν	^{40}K	He(s),C,Ne	^{60}Ni	α, He(s)
^{16}O	He	^{41}K	xO	^{61}Ni	He(s),α,Ia-det
^{17}O	novae, L*	^{40}Ca	xO,O	^{62}Ni	He(s),α
^{18}O	He	^{42}Ca	xO	^{64}Ni	He(s)
^{19}F	ν,He,L*	^{43}Ca	C,Ne,α	^{63}Cu	He(s),C,Ne
^{20}Ne	C	^{44}Ca	α,Ia-det	^{65}Cu	He(s)
^{21}Ne	C	^{46}Ca	C,Ne	^{64}Zn	ν-wind,α,He(s)
^{22}Ne	He	^{48}Ca	nse-IaMCh	^{66}Zn	He(s),α,nse-IaMCh
^{23}Na	C,Ne,H	^{45}Sc	α,C,Ne,ν	^{67}Zn	He(s)
^{24}Mg	C,Ne	^{46}Ti	xO,Ia-det	^{68}Zn	He(s)
^{25}Mg	C,Ne	^{47}Ti	Ia-det,xO,xSi	r	ν-wind
^{26}Mg	C,Ne	^{48}Ti	xSi,Ia-det	p	xNe,O
^{27}Al	C,Ne	^{49}Ti	xSi	s(A<90)	He(s)
^{28}Si	xO,O	^{50}Ti	nse-IaMCh,He(s)	s(A>90)	L*
^{29}Si	C,Ne	^{50}V	C,Ne,xNe,xO		

plosion as a supernova. Table III summarizes our best estimates of where each isotope of the elements lighter than zinc has been created in Nature. We adopt as our standard the composition of the sun.

In this table, "BB" stands for the big bang. Stable isotopes of both hydrogen and ^{3}He, most of ^{4}He, and some ^{7}Li were made there (see, for example Walker *et al.*, 1991; Olive, Steigman, and Walker, 2000). "CR" is for cosmic-ray spallation, responsible for some of the rarest, most fragile isotopes in nature, ^{6}Li, ^{9}Be, and ^{10}B (Fields and Olive, 1999; Fields *et al.*, 2000; Ramaty *et al.*, 2000). Other light isotopes, especially ^{11}B, ^{19}F, and some ^{7}Li, are made by the neutrino process in massive stars (Sec. VIII.B.4). "L" here, means that the isotope is synthesized in stars lighter than $8M_{\odot}$. Notable examples are most of ^{13}C and ^{14}N (Renzini and Voli, 1981), half or more of ^{12}C (Timmes, Woosley, and Weaver, 1995), and the s process above mass 90 (Renzini and Voli, 1981; Meyer, 1994; Busso *et al.*, 2001).

Type-Ia supernovae are responsible for making part of the iron group (including about one-half of ^{56}Fe; Thielemann, Nomoto, and Yokoi, 1986; Timmes, Woosley, and Weaver, 1995). Rare varieties of type-Ia supernovae may be necessary for the production of a few isotopes not adequately made elsewhere. These include neutron-rich isotopes of Ca, Ti, Cr, and Fe made in accreting white dwarfs that ignite carbon deflagration at densities so high that they almost collapse to neutron stars (Woosley, 1997; Iwamoto *et al.*, 1999). We call these "nse-IaMCh" for carbon deflagrations in white dwarfs very near the Chandrasekhar mass. Temperatures near 10^{10} K assure nuclear statistical equilibrium and densities near 6×10^{9} g cm^{-3} cause electron capture until $Y_e \approx 0.42$. Another rare variety of type-Ia supernovae are the helium detonations ("Ia-det"; Woosley and Weaver, 1995). These give temperatures of billions of K in helium-rich zones and may be necessary in order to understand the relatively large solar abundance of ^{44}Ca (made in supernovae as radioactive ^{44}Ti) only in regions of high temperature and large helium mass fraction. This may also explain the production of a few other rare isotopes like ^{43}Ca and ^{47}Ti. Classical novae seem necessary to explain the origin of ^{15}N (in the beta-limited CNO cycle) and ^{17}O (Jose and Hernanz, 1998). Prior to 1995, ^{17}O was regarded as a product of massive stars (Woosley and Weaver, 1995).

All the other labels in Table III refer to burning stages in massive stars: "He" for helium burning, "C" for carbon burning, etc. An "x" in front of the elemental symbol indicates that the burning is of the explosive variety, not the presupernova evolution in hydrostatic equilibrium. "α" stands for the α-rich freeze-out from nuclear statistical equilibrium (Woosley, Arnett, and Clayton, 1973) and ν wind is the neutrino-powered wind (Sec.

OTHER PROCESSES

ν - PROCESS

νp - PROCESS

r - PROCESS [?]

p - PROCESS [?]

} LATER

ν-PROCESS

- NOT RELATED TO SHOCK BUT DRIVEN BY PASSAGE OF ν's THRO' STAR
- ν's { VERY SMALL N(ν) FLUX VERY HIGH for a SHORT TIME

→ MAY ACCOUNT FOR RARE SPECIES CREATED FROM ABUNDANT TARGETS

N.B. EARLY PAPER TITLED NEUTRINO-INDUCED N' SYNTHESIS AND ! DEUTERIUM

WOOSLEY, 1977, NATURE 269, 42

Examples:

^{19}F from $^{20}Ne(\nu_x, \nu_x' p)^{19}F$

$^{20}Ne(\nu_x, \nu_x' n)^{19}Ne(e^+\nu)^{19}F$

^{7}Li via $^{4}He(\nu_x, \nu_x' n)^{3}He(\alpha,\gamma)^{7}Be \rightarrow {}^{7}Li$

^{11}B from ^{12}C

^{138}La from ^{138}Ba

$^{180}Ta^m$ from ^{182}Hf, ^{181}Hf, ^{182}W

$(\nu_e, e^- 2n)$ $(\nu_e, e^- n)$ $(\bar{\nu}_e, e^+ 2n)$

rarest naturally occurring nuclide

$t_{1/2} \sim 10^{16}$ yrs

with

^{180}Ta $t_{1/2} \sim 8$ hours

PROMISING - no direct/indirect proof

The νp-process

- Not shock-related
- Occurs near proto-NS

$T > 10^{10}$ K

Sea of p and n

but

$\nu_e + n \Leftrightarrow p + e^-$

$\bar{\nu}_e + p \Leftrightarrow n + e^+$ $\Big\rangle$ $p/n > 1$ because of n-p mass difference

assume ν_e, $\bar{\nu}_e$ flux and spectra are identical

$T < 10^{10}$ K on cooling

$p, n \rightarrow \alpha$, then αs $\rightarrow {}^{12}C$ and further α capture

get to ${}^{56}Ni$, ${}^{60}Zr$, ${}^{64}Ge$ ($N=Z$)

waiting points (β^+ decay)

But unlike rp-process, waiting points can be bypassed as in
$^{64}Ge(n,p)^{64}Ga$

May account for Mo, Ru light p nuclei = otherwise a problem (see p process discussion)

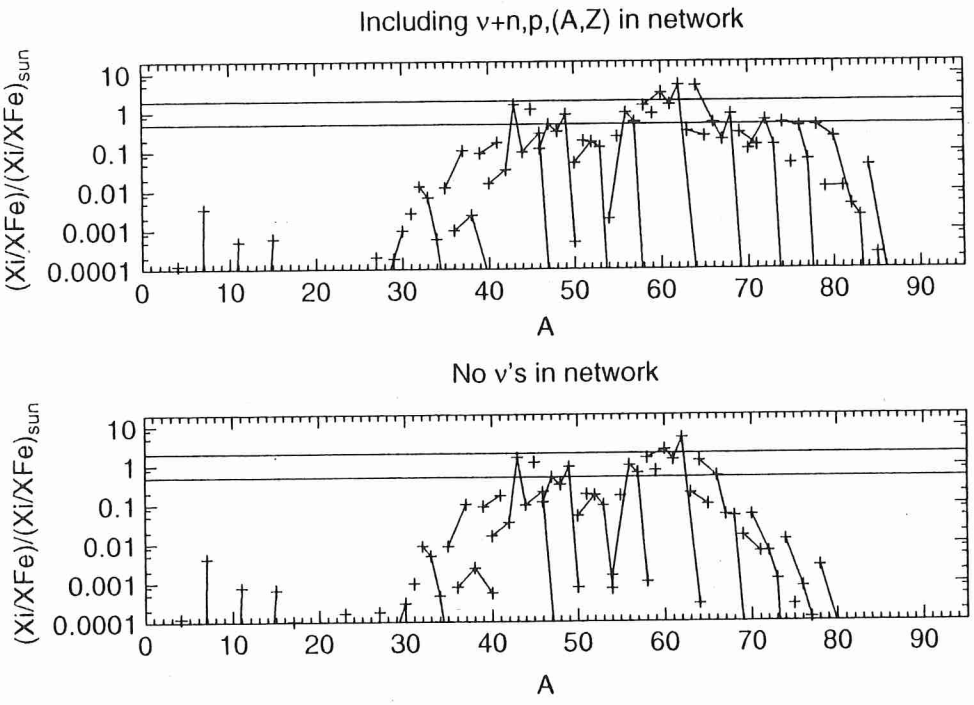

Fig. 4.17 Final abundances in mass zones in the innermost ejecta which experienced neutrino irradiation, leading to proton-rich conditions ($Y_e > 0.5$). The *bottom part* of the figure shows the neucleosynthesis results in the innermost ejecta of explosive, after alpha-rich and proton-rich freeze-out from Si-burning, normalized to solar after decay. The *top part* of the figure also includes the interaction of anti-electron neutrinos with protons ($\bar{\nu}_e + p \rightarrow n + e^+$) which produces neutrons, permitting the late change of ^{64}Ge via ^{64}Ge$(n, p)^{64}$Ga. This feature permits further proton captures to produce havier nuclei (the so-called νp process). Here matter up to $A = 85$ is produced

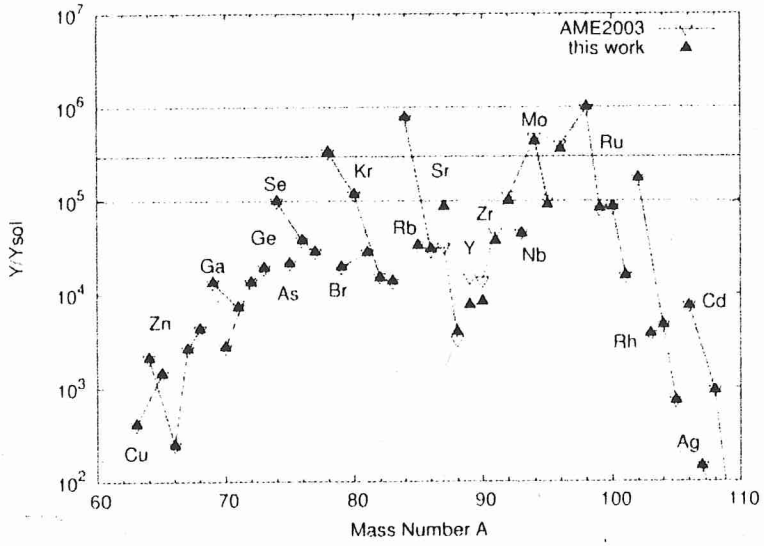

Fig. 4.18 Final abundances in mass zones experiencing the νp process, i.e. the innermost ejecta of explosive, alpha-rich freeze-out Si-burning, normalized to solar after decay for two sets of thermonuclear reaction rates/masses. Matter up to $A = 100$ can be produced easily